Generalized susceptibility of a quasi-one-dimensional system with periodic potential: A model for the organic superconductor $(TMTSF)_2ClO_4$

Yasumasa Hasegawa[1] and Keita Kishigi[2]
[1]*Department of Material Science, Graduate School of Material Science, University of Hyogo, Hyogo 678-1297, Japan*
[2]*Faculty of Education, Kumamoto University, Kurokami 2-40-1, Kumamoto, 860-8555, Japan*
(Received 15 May 2008; published 25 July 2008)

The nesting vector and the magnetic susceptibility of the quasi-one-dimensional system having imperfectly nested Fermi surface are studied analytically and numerically. The magnetic susceptibility has the plateaulike maximum in *sweptback* region in the momentum space, which is surrounded by $\mathbf{Q}=(2k_F,\pi)+\mathbf{q}_i$ (k_F is the Fermi wave number $i=1,3,4$ and $\mathbf{q}_1$, $\mathbf{q}_3$, and $\mathbf{q}_4$ are given in this paper). The best nesting vector, at which the susceptibility $\chi_0(\mathbf{Q})$ has the absolute maximum at $T=0$, is obtained near but not at the inflection point $\mathbf{Q}=(2k_F,\pi)+\mathbf{q}_4$. The effect of the periodic potential V on the susceptibility is studied, which is important for the successive transitions of the field-induced spin-density wave in $(TMTSF)_2ClO_4$. We obtain that the sweptback region (surrounded by $\mathbf{q}_2$, $\mathbf{q}_3$, and $\mathbf{q}_4$ when $V>0$) becomes small as V increases and it shrinks to $\mathbf{q}_3$ for $V\geq 4t_b'$, where t_b' gives the degree of imperfect nesting of the Fermi surface, i.e., the second harmonics of the warping in the Fermi surface. The occurrence of the sign reversal of the Hall coefficient in the field-induced spin-density wave states is discussed to be possible only when $V<2t_b'-2t_4$, where t_4 is the amplitude of the fourth harmonics of the warping in the Fermi surface. This gives the limitation for the magnitude of V.

DOI: 10.1103/PhysRevB.78.045117 PACS number(s): 75.30.Fv, 78.30.Jw, 71.10.Pm

I. INTRODUCTION

Various interesting properties, such as field-induced spin-density wave (FISDW), quantum Hall effect, and superconductivity have been observed in the quasi-one-dimensional (Q1D) organic conductors, $(TMTSF)_2X$, where X is PF_6, ClO_4, etc.[1] The successive transitions between the different FISDW phases occur as the magnetic field is increased. The FISDW has been understood as a consequence of the reduction in the dimensionality due to the magnetic field and the quantization of the nesting vector.[2–11] The FISDW phases are characterized by the integer N, by which the wave number of FISDW is given as $Q_x=2k_F+NG$, where k_F is the Fermi wave number, $G=beB/\hbar$, b is the lattice constant (we take $b=1$ in this paper), e is the electron charge, B is the magnetic field, and $\hbar=h/2\pi$ (h is the Planck constant). We take $\hbar=1$ hereafter in this paper. The Hall conductivity is quantized as $\sigma_{xy}=2Ne^2/h$ with the quantum number N of the nesting vector.[12–14] The quantization of the x component of the nesting vector Q_x can be seen as the sharp peaks in the susceptibility for the noninteracting system $\chi_0(\mathbf{Q})$ at $Q_x=2k_F+NG$ in the magnetic field.

The peaks of $\chi_0(\mathbf{Q})$ in the magnetic field can be understood to some extent by the peaks of $\chi_0(\mathbf{Q})$ in the absence of the magnetic field. If the nesting of the Fermi surface is perfect, $\chi_0(\mathbf{Q})$ in the absence of the magnetic field diverges at the nesting vector as temperature becomes zero. In that case the successive transitions of FISDW does not happen. If the nesting of the Fermi surface is not perfect, the best nesting vector at $B=0$, which gives the maximum of $\chi_0(\mathbf{Q})$, is located in the reciprocal space at

$$\mathbf{Q}=\mathbf{Q}_0+\mathbf{q}, \tag{1}$$

where

$$\mathbf{Q}_0=(2k_F,\pi), \tag{2}$$

and $\mathbf{q}\neq 0$. If $q_x>0$, the quantum number N of FISDW is positive. If $q_x<0$ at the best nesting vector, however, the negative N is possible in some region of the magnetic field.[15] The umklapp scattering has been proposed as the alternative explanation for the negative N (Ref. 16). We do not consider the umklapp scattering in this paper.

Although $(TMTSF)_2PF_6$ is well understood by the quasi-one-dimensional model, $(TMTSF)_2ClO_4$ is a little more complicated. Below $T_{AO}\approx 24$ K the anion ClO_4 (which has no inversion symmetry) orders alternatively in the y direction, resulting the periodic potential V in the electron system. Actually, the magnetic field and temperature phase diagram in $(TMTSF)_2PF_6$ (Refs. 17–21) is different from that in $(TMTSF)_2ClO_4$ (Refs. 22–24). The origin of the different phase diagrams in $(TMTSF)_2PF_6$ and $(TMTSF)_2ClO_4$ is caused by the periodic potential V. The magnitude of V is first estimated to be of the order of $T_{AO}=24$ K, i.e., $V\ll t_b$ (Refs. 25 and 26). The suppression of the $N=0$ FISDW state[25] and even-N FISDW states[26] has been shown by the perturbation in V. On the other hand, the magnitude of V has been estimated to be $V=0.83t_b$ from the angle dependence of the magnetoresistance by Yoshino *et al.*[27] By treating V not in perturbation, a lot of interesting features, such as existence of several nesting vectors[28–31] and the phase diagram of the FISDW states,[32,33] has been obtained. Recently, Yoshino *et al.*[34] has estimated the value to be $V=0.028t_a$ ($V=0.34t_b$ with their estimation $t_a=12t_b$). Lebed *et al.*[35,36] have estimated the value as $V=0.2t_b$. The estimation of V is given in this paper from the existence of the sign reversal of the Hall effect.

In this paper, we study the nesting vector and the susceptibility in the quasi-one-dimensional system with imperfectly nested Fermi surface in the absence of the magnetic field. The analytical expression of the susceptibility and the nearly flat region in the reciprocal space is given analytically in the

 ©2008 The American Physical Society

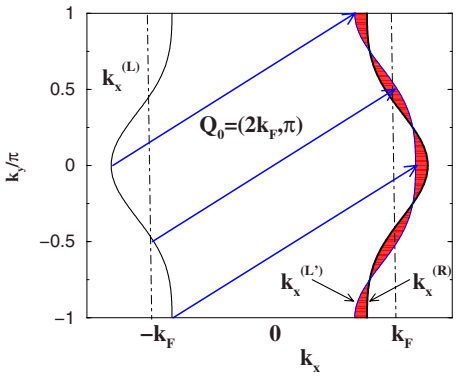

FIG. 1. (Color online) Fermi surface for $V=0$.

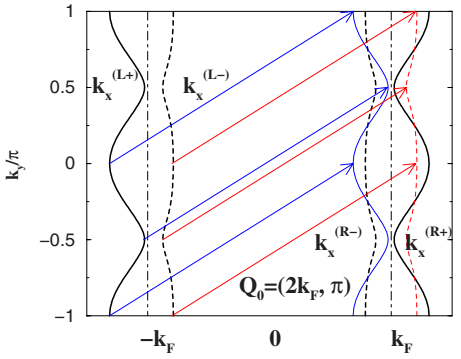

FIG. 2. (Color online) Fermi surface for $V\neq 0$.

simple model with $V=0$. The effect of V on the nesting vector and the susceptibility are studied in detail numerically. Although we consider the zero magnetic-field case, we hope that the obtained results are valid in a finite magnetic-field case.

II. MODEL

We neglect the small dispersion in the k_z direction and study the tight-binding model in the square lattice with anisotropic transfer integral elements $t_a \gg t_b$. We take the lattice constant to be one. In the real system, the crystal is triclinic and we have to consider the multiple-transverse-transfer integrals;[37] but most of the essential features are obtained by studying the simple model in the square lattice.[1] The energy dispersion can be linearized with respect to k_x and we take account the higher harmonic terms for k_y as

$$\epsilon(\mathbf{k}) = v_F(|k_x| - k_F) + t_\perp(k_y), \tag{3}$$

where

$$t_\perp(k_y) = -2t_b \cos k_y - 2t_b' \cos(2k_y) - 2t_3 \cos(3k_y) - 2t_4 \cos(4k_y) \tag{4}$$

and we study the case t_b, t_b', t_3, and t_4 to be positive. The terms proportional to t_3 and t_4 are thought to be essential[15,33] to understand the negative N phase[38,39] of FISDW in some region of the magnetic field. The Fermi surface consists of two "Fermi lines" near $k_x \approx \pm k_F$ as shown in Fig. 1. The Fermi surface is almost nested, i.e., when we translate the left part of the Fermi line with the vector $\mathbf{Q} \approx \mathbf{Q}_0$, it overlaps with the right part of the Fermi line; but the overlap is not perfect due to the t_b' and t_4 terms.

The Brillouin zone is divided into halves in the k_y direction by the periodic potential. The Hamiltonian is written as a 2×2 matrix with the anion potential V as

$$\mathcal{H} = \begin{pmatrix} \epsilon(\mathbf{k}) & V \\ V & \epsilon(\mathbf{k}+\mathbf{Q}_A) \end{pmatrix}, \tag{5}$$

where $\mathbf{Q}_A=(0,\pi)$. The energy $E(\mathbf{k})$ is given by

$$E(\mathbf{k}) = \frac{1}{2}(\epsilon(\mathbf{k}) + \epsilon(\mathbf{k}+\mathbf{Q}_A) \pm \sqrt{[\epsilon(\mathbf{k}) - \epsilon(\mathbf{k}+\mathbf{Q}_A)]^2 + 4V^2}), \tag{6}$$

and the Fermi surface consists of four lines as shown in Fig. 2.

It is known[28] that the susceptibility $\chi_0(\mathbf{Q})$ has the maximum near $\mathbf{Q} \approx \mathbf{Q}_0$ if $V \lesssim 1.5t_b$ when $t_b'=0.1t_b$ (i.e., $V \lesssim 15t_b'$), while the absolute maximum of $\chi_0(\mathbf{Q})$ is located near $\mathbf{Q} \approx (2k_F \pm 2V/v_F, \pi/2)$ if $V \gtrsim 1.5t_b$. The peak of $\chi_0(\mathbf{Q})$ near $\mathbf{Q} \approx \mathbf{Q}_0$ is caused by the nesting between the outer Fermi surface and the inner Fermi surface ($\mathbf{k}_x^{(R+)}$ and $\mathbf{k}_x^{(L-)}$), i.e., the red and blue arrows in Fig. 2, while the peaks of $\chi_0(\mathbf{Q})$ near $\mathbf{Q} \approx (2k_F \pm 2V/v_F, \pi/2)$ are caused by the nesting of the outer Fermi surfaces [$\mathbf{k}_x^{(R+)}$ and $\mathbf{k}_x^{(L+)}$] or the inner Fermi surfaces [$\mathbf{k}_x^{(R-)}$ and $\mathbf{k}_x^{(L-)}$] (Refs. 32, 40, and 41). The maximum value of $\chi_0(\mathbf{Q})$ near $\mathbf{Q} \approx \mathbf{Q}_0$ depends weakly on V if $V \lesssim 0.4t_b$, and it decreases as V increases if $V \gtrsim 0.4t_b$. Sengupta and Dupuis[29] and Zanchi and Bjelis[30] obtained similar results.

In this paper we examine in detail the nesting properties of the quasi-one-dimensional systems without and with the periodic potential ($V \lesssim 0.5t_b$). Thus we focus on the nesting condition for only $\mathbf{Q} \approx \mathbf{Q}_0$.

III. NESTING OF THE FERMI SURFACE FOR $V=0$

In this section we study the nesting properties of the quasi-one-dimensional system described by Eq. (3). The Fermi surface consists of two curves (see Fig. 1). The right and left parts of the Fermi surface are given as a function of k_y,

$$k_x^{(R)}(k_y) = k_F - \frac{1}{v_F} t_\perp(k_y), \tag{7}$$

$$k_x^{(L)}(k_y) = -k_F + \frac{1}{v_F} t_\perp(k_y). \tag{8}$$

We translate the left part of the Fermi surface with the nesting vector $\mathbf{Q}=\mathbf{Q}_0+\mathbf{q}$. The translated curve is given by

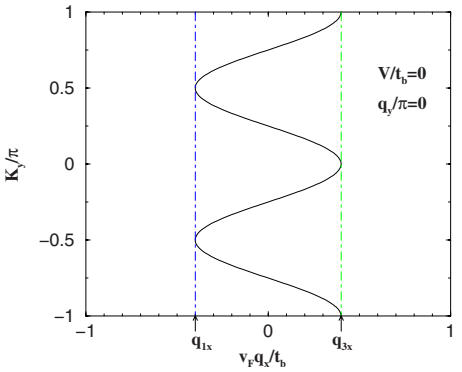

FIG. 3. (Color online) q_x vs K_y (Eq. (11)) for $q_y=0$ and $q_y=\pi$.

$$k_x^{(L')}(k_y) = k_F + q_x + \frac{1}{v_F} t_\perp (k_y + q_y + \pi). \tag{9}$$

The difference between the right part of the Fermi surface and the translated left part of the Fermi surface is given by

$$k_x^{(L')}(k_y) - k_x^{(R)}(k_y) = q_x + \frac{1}{v_F}[t_\perp(k_y) + t_\perp(k_y + q_y + \pi)]. \tag{10}$$

If $t_b'=t_4=0$, the nesting of the Fermi surface is perfect with $q_x=q_y=0$, i.e., $k_x^{(L')}(k_y)-k_x^{(R)}(k_y)=0$ for all values of k_y. If $t_b' \neq 0$ or $t_4 \neq 0$, the nesting of the Fermi surface is not perfect. In this case the Fermi surface intersects with the translated one with the nesting vector $\mathbf{Q}_0+\mathbf{q}$, if q_x and q_y satisfy

$$\begin{aligned} q_x &= \frac{-1}{v_F}[t_\perp(k_y) + t_\perp(k_y + q_y + \pi)] \\ &= \frac{4}{v_F}\left[t_b \sin(K_y)\sin\left(\frac{q_y}{2}\right) + t_b' \cos(2K_y)\cos(q_y) \right. \\ &\quad \left. + t_3 \sin(3K_y)\sin\left(\frac{3q_y}{2}\right) + t_4 \cos(4K_y)\cos(2q_y) \right], \end{aligned} \tag{11}$$

for some value of K_y, where

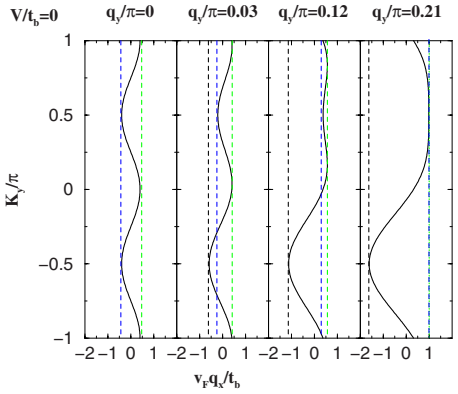

FIG. 4. (Color online) q_x vs K_y [Eq. (11)] for some values of q_y. There are two minimums $[q_x^{\min(\pm)}(q_y)]$ and one maximum $[q_x^{\max}(q_y)]$ of q_x as a function of K_y for each $0<|q_y|<q_{4y}$, while only one minimum and one maximum of q_x for $|q_y|>q_{4y}$ as shown by the dotted vertical lines.

$$K_y = k_y + \frac{q_y}{2}. \tag{12}$$

Equation (11) is the condition for the nesting vector ($\mathbf{Q}=\mathbf{Q}_0+\mathbf{q}$) to realize the intersection of the translated left part of the Fermi surface with the right part of the Fermi surface at k_y. In Fig. 3 we plot q_x vs K_y for $q_y=0$. We define two vectors, $\mathbf{q}_1$ and $\mathbf{q}_3$, as $q_{1y}=q_{3y}=0$ and q_{1x} and q_{3x} being the minimum and the maximum of q_x as a function of K_y at $q_y=0$, respectively. When $t_4 \leq t_b'/4$ (in this paper we study only in this case), the maximum of q_x as a function of K_y for $q_y=0$ is given at $K_y=0$ and $\pm\pi$, and the minimum of q_x as a function of K_y for $q_y=0$ is given at $K_y=\pm\pi/2$ as shown in Fig. 3;

$$\mathbf{q}_1 = \left(\frac{4}{v_F}(-t_b' + t_4), 0\right), \tag{13}$$

$$\mathbf{q}_3 = \left(\frac{4}{v_F}(t_b' + t_4), 0\right). \tag{14}$$

We define $\mathbf{q}_2=\mathbf{q}_1$ for $V=0$ and we will define $\mathbf{q}_2$ for $V\neq 0$ in Sec. V.

We plot q_x vs K_y [Eq. (11)] for some values of q_y in Fig. 4. As seen in Fig. 4, q_x as a function of K_y has two minimums at $K_y=\pm\pi/2$ $[q_x^{\min(\pm)}(q_y)]$ and one maximum at $0 \leq K_y \leq \pi/2$ $[q_x^{\max}(q_y)]$ if $0<|q_y|<q_{4y}$ ($\mathbf{q}_4$ will be given later). There is one minimum at $K_y=-\pi/2$ and one maximum at $K_y=\pi/2$ if $|q_y|>q_{4y}$. We obtain $q_x^{\min(+)}(q_y)$ and $q_x^{\min(-)}(q_y)$ as

$$q_x^{\min(+)}(q_y) = \frac{4}{v_F}\left(-t_b' \cos q_y + t_b \sin\frac{|q_y|}{2} - t_3 \sin\frac{3|q_y|}{2} + t_4 \cos 2q_y\right), \tag{15}$$

$$q_x^{\min(-)}(q_y) = \frac{4}{v_F}\left(-t_b' \cos q_y - t_b \sin\frac{|q_y|}{2} + t_3 \sin\frac{3|q_y|}{2} + t_4 \cos 2q_y\right). \tag{16}$$

If t_3 and t_4 are finite, we have to solve the fourth-degree equation to obtain the expression of $q_x^{\max}(q_y)$, but it is easy to obtain $q_x^{\max}(q_y)$ numerically. We define $\mathbf{q}_4=(q_{4x},q_{4y})$ by the equation

$$q_x^{\min(+)}(q_{4y}) = q_x^{\max}(q_{4y}) = q_{4x}. \tag{17}$$

If $t_3=t_4=0$, the simple expressions of $q_x^{\max}(q_y)$ and $\mathbf{q}_4$ are obtained as

$$q_x^{\max}(q_y) = \frac{4}{v_F}\left(t_b' \cos q_y + \frac{t_b^2 \sin^2\frac{q_y}{2}}{8t_b' \cos q_y}\right), \tag{18}$$

$$q_{4x} = \frac{1}{v_F}\frac{24t_b'}{\sqrt{1+128\left(\frac{t_b'}{t_b}\right)^2}+1}, \tag{19}$$

and

$$q_{4y} = \pm 2 \sin^{-1}\left[\frac{8\frac{t_b'}{t_b}}{\sqrt{1+128\left(\frac{t_b'}{t_b}\right)^2}+1}\right]. \tag{20}$$

Note that $q_x^{\max}(q_y)$ has the physical meaning only if $|q_y| \le q_{4y}$, since the analytical form [Eq. (18)] obtained from the

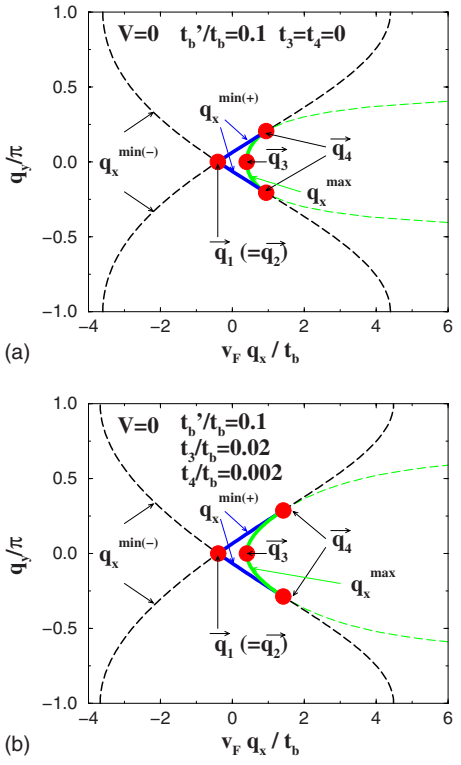

FIG. 5. (Color online) $q_x^{\min(-)}(q_y)$ (dashed lines in $q_x<q_{1x}$), $q_x^{\min(+)}(q_y)$ (thick blue lines in $q_{1x}<q_x<q_{4x}$ and dashed lines in $q_x>q_{4x}$), and $q_x^{\max}(q_y)$ (thick green lines in $q_{3x}<q_x<q_{4x}$ and dashed green lines in $q_x>q_{4x}$). We take $t_b'/t_b=0.1$ and $t_3=t_4=0$ (upper figure) and $t_3/t_b=0.02$ and $t_4/t_b=0.002$ (lower figure). In the *sweptback* region enclosed by $\mathbf{q}_1$, $\mathbf{q}_3$, and $\mathbf{q}_4$, $\chi_0(\mathbf{Q})$ has large values.

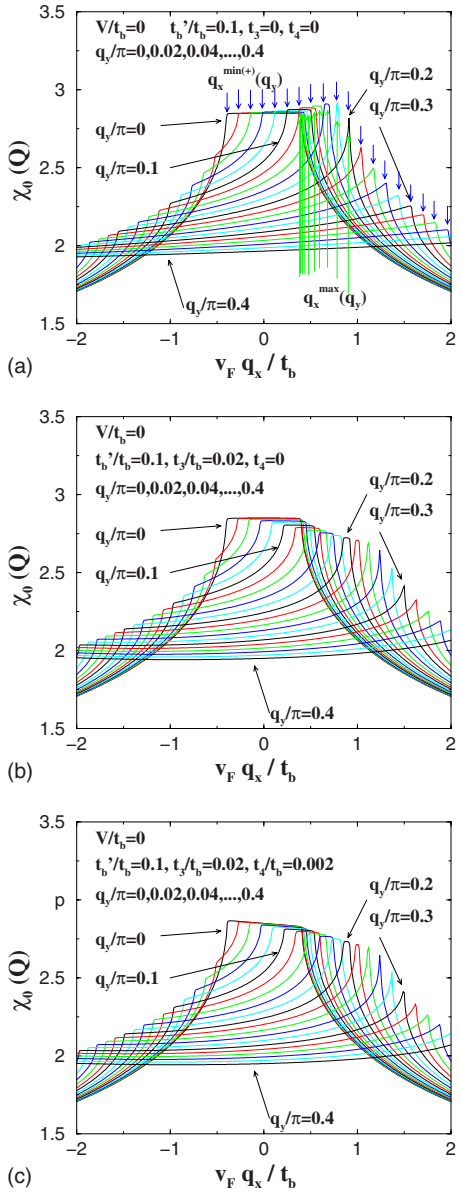

FIG. 6. (Color online) $\chi_0(\mathbf{Q})$ at $T=0$ (Eq. (22)) as a function of q_x. We take $t_b'/t_b=0$ and $t_3=t_4=0$ (upper figure); $t_3/t_b=0.02$ and $t_4=0$ (middle figure); and $t_3/t_b=0.02$ and $t_4/t_b=0.002$ (lower figure). As obtained by Zanchi and Montambaux (Ref. 15), t_3 reduces the peak height near $\mathbf{q}_4$ and t_4 lifts the degeneracy at $\mathbf{q}_1$ and $\mathbf{q}_3$.

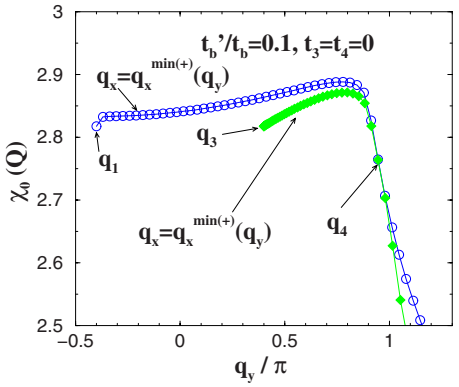

FIG. 7. (Color online) $\chi_0(\mathbf{Q})$ at $T=0$ (Eq. (22)) as a function of q_x for (q_x,q_y) on the curves $(q_x^{\min(+)}(q_y),q_y)$ (filled green diamonds) and $(q_x^{\max}(q_y),q_y)$ (open blue circles) in Fig. 5. For $q_x>q_{4x}$, we use Eq. (18), although curves $(q_x^{\max},q_y)$ terminate at $\mathbf{q}=\mathbf{q}_4$. Note that the absolute maximum is not realized at (q_{4x},q_{4y}). We take $t_b'/t_b=0.1$ and $t_3=t_4=0$.

case of $t_3=t_4=0$ and the numerically obtained values at $|q_y|>q_{4y}$ corresponds to the local maximum of q_x as a function of $\sin(K_y/2)$ at $|\sin(K_y/2)|>1$. We plot $q_x^{\max}(q_y)$, $q_x^{\min(+)}(q_y)$, and $\mathbf{q}_i$ ($i=1$, 3, and 4) in Fig. 5. There is a large overlap between the Fermi line and the translated one if $\mathbf{q}$ is in the *sweptback* region with the apexes $\mathbf{q}_1$ and $\mathbf{q}_4$ enclosed by the thick lines in Fig. 5.

IV. SUSCEPTIBILITY IN THE Q1D SYSTEM WITH $V=0$

The susceptibility

$$\chi_0(\mathbf{Q})=\sum_{\mathbf{k}}\frac{f(E_{\mathbf{k}+\mathbf{Q}})-f(E_{\mathbf{k}})}{E_{\mathbf{k}}-E_{\mathbf{k}+\mathbf{Q}}}, \tag{21}$$

where $f(E_{\mathbf{k}})$ is the Fermi distribution function, is calculated at $T=0$ as

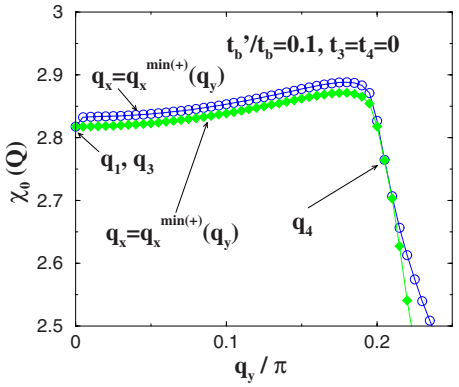

FIG. 8. (Color online) $\chi_0(\mathbf{Q})$ at $T=0$ (Eq. (22)) as a function of q_y for (q_x,q_y) on the curves $(q_x^{\min(+)}(q_y),q_y)$ (filled green diamonds) and $(q_x^{\max}(q_y),q_y)$ (open blue circles) in Fig. 5. We take $t_b'/t_b=0.1$ and $t_3=t_4=0$.

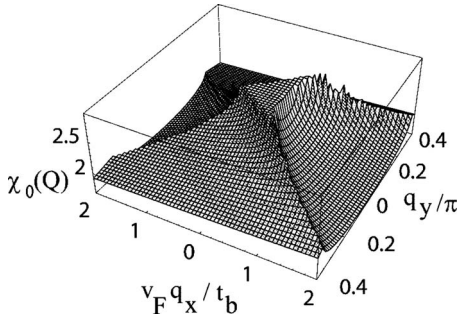

FIG. 9. 3D plot of $\chi_0(\mathbf{Q})$ at $T=0$ (Eq. (22)) as a function of q_x and q_y. We take $t_b'/t_b=0.1$ and $t_3=t_4=0$.

$$\begin{aligned}\chi_0(\mathbf{Q})&=\int_{-\pi}^{\pi}\frac{dk_y}{2\pi}\int_{k_x^{(L)}(k_y)}^{k_x^{(R)}(k_y)}\frac{dk_x}{2\pi}\frac{2}{\epsilon(\mathbf{k}-\mathbf{Q})-\epsilon(\mathbf{k})}\\&=\frac{1}{\pi}\int_{-\pi}^{\pi}\frac{dk_y}{2\pi}\left[\int_{k_x^{(L)}(k_y)}^{0}\frac{dk_x}{v_FQ_x+t_\perp(k_y-Q_y)-t_\perp(k_y)}\right.\\&\left.+\int_{0}^{k_x^{(R)}(k_y)}\frac{dk_x}{v_F(-2k_x+Q_x)+t_\perp(k_y-Q_y)-t_\perp(k_y)}\right]\\&=\frac{1}{2\pi v_F}\int_{-\pi}^{\pi}\frac{dk_y}{2\pi}\left[\frac{v_Fk_F-t_\perp(k_y)}{v_FQ_x+t_\perp(k_y-Q_y)-t_\perp(k_y)}\right.\\&\left.-\frac{1}{2}\log\left|\frac{v_F(Q_x-2k_F)+t_\perp(k_y-Q_y)+t_\perp(k_y)}{v_FQ_x+t_\perp(k_y-Q_y)-t_\perp(k_y)}\right|\right].\end{aligned} \tag{22}$$

The susceptibility is finite at $T=0$ and has the singularity (kinks) as a function of $\mathbf{Q}$. The singularity of $\chi_0(\mathbf{Q})$ comes from the integration of the logarithmic term in Eq. (22). For $Q_y=\pi$ (i.e., $q_y=0$) and $t_3=t_4=0$, the singular part of $\chi_0(\mathbf{Q}_0+\mathbf{Q})$ is calculated as

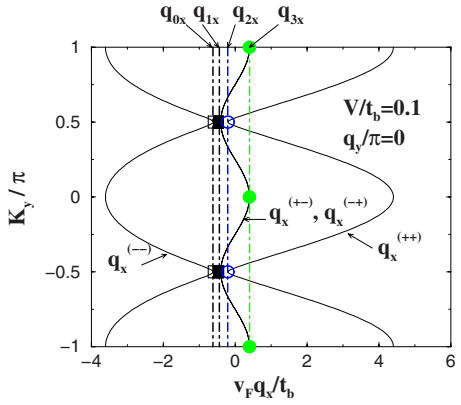

FIG. 10. (Color online) q_x vs K_y [Eq. (27)] for $q_y=0$ and $V/t_b=0.1$.

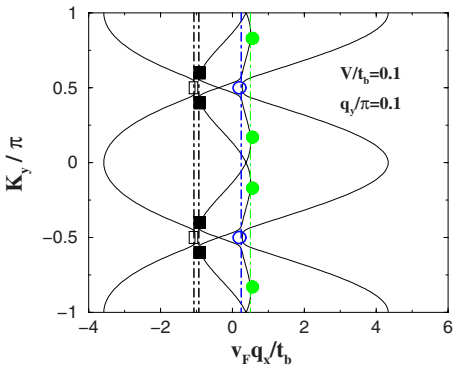

FIG. 11. (Color online) q_x as a function of K_y for $q_y/\pi=0.1$.

$$\chi_{0,\mathrm{sing}} = \frac{1}{\pi v_F}\int_{-\pi}^{\pi}\frac{dk_y}{2\pi}\left(-\frac{1}{2}\right)\log\left|\frac{v_F q_x - 4t_b'\cos 2k_y}{2k_F v_F}\right|$$

$$= \begin{cases} -\dfrac{1}{2\pi v_F}\log\left|\dfrac{q_x v_F + \sqrt{(q_x v_F)^2-(4t_b')^2}}{4k_F v_F}\right| \\ \text{if } |q_x v_F| > 4t_b' \\ -\dfrac{1}{2\pi v_F}\log\left|\dfrac{t_b'}{k_F v_F}\right| \\ \text{if } |q_x v_F| < 4t_b' \end{cases} . \tag{23}$$

It is obtained from Eq. (23) that $\chi_0(\mathbf{q})$ has a plateau as a function of q_x when $t_3=t_4=0$ and $q_y=0$. If t_3, t_4, and q_y are not zero, we have to integrate Eq. (22) numerically. In Fig. 6 we plot $\chi_0(\mathbf{Q})$ for several t_3, t_4, and q_y as a function of q_x. It can be seen that if $t_3=t_4=0$, nearly flat peak at $q_x^{\min(+)}(q_y)<q_x<q_x^{\max}$ first increases as q_y increases, and it has the absolute maximum before q_y reaches q_{4y} ($=0.2065\pi$ and $v_F q_{4x}/t_b=0.956$ when $t_b'/t_b=0.1$) as shown in the top figure in Fig. 6. If $t_3>0$, the peaks for $q_y\neq 0$ are suppressed as shown in the middle figure in Fig. 6. If $t_4>0$, the degeneracy of $\chi_0(\mathbf{Q}_0+\mathbf{Q})$ at $\mathbf{q}_1$ and $\mathbf{q}_3$ is lifted and the absolute maximum of $\chi_0(\mathbf{Q}_0+\mathbf{q})$ is obtained at $\mathbf{q}_1$ for the sufficiently large values of t_3 and t_4 as seen in the bottom figure in Fig. 6.

As seen in Fig. 6, $\chi_0(\mathbf{Q}_0+\mathbf{q})$ has a plateaulike maximum in the region $q_x^{\min(+)}(q_y)<q_x<q_x^{\max}(q_y)$. The absolute maximum of $\chi_0(\mathbf{Q}_0+\mathbf{q})$ occurs at $\mathbf{q}$ close to $\mathbf{q}_4$ but not at $\mathbf{q}=\mathbf{q}_4$ as seen in Figs. 7 and 8, where we plot $\chi_0(\mathbf{Q}_0+\mathbf{q})$ as a function of q_x or q_y on the curves of $q_x=q_x^{\min(+)}(q_y)$ and $q_x=q_x^{\max}(q_y)$, respectively. The three-dimensional plot of $\chi_0(\mathbf{Q}_0+\mathbf{q})$ is shown in Fig. 9. When $t_3=t_4=0$ and $q_y=q_{4y}$, Eq. (11) becomes

$$q_x = \frac{1}{k_F}\frac{4t_b'\left[6-16\sin^4\left(K_y-\frac{\pi}{2}\right)\right]}{\sqrt{1+128\left(\frac{t_b'}{t_b}\right)^2}+1}. \tag{24}$$

Therefore, q_x as a function of K_y has a maximum at $K_y=\pi/2$ as $q_x\propto 6-16(K_y-\pi/2)^4$ when $q_y=q_{4y}$. With the vector $\mathbf{Q}=\mathbf{Q}_0+\mathbf{q}_4$ the nesting of the Fermi surface is better than other $\mathbf{q}$'s, which will make the expectation of the large $\chi_0(\mathbf{Q}_0+\mathbf{q})$. However, the region of q_y [where $\chi_0(\mathbf{Q}_0+\mathbf{q})$ is mainly contributed] is larger at $q_x\lesssim q_{4x}$ and $|q_y|\lesssim q_{4y}$ than at $\mathbf{q}=\mathbf{q}_4$. This is the reason why the absolute maximum of $\chi_0(\mathbf{Q}_0+\mathbf{q})$ is not located at the inflection point ($\mathbf{q}=\mathbf{q}_4$).

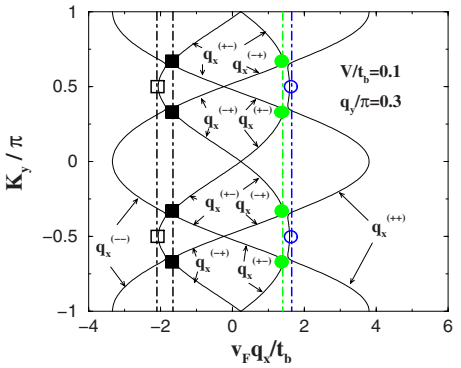

FIG. 12. (Color online) q_x as a function of K_y for $q_y/\pi=0.3$.

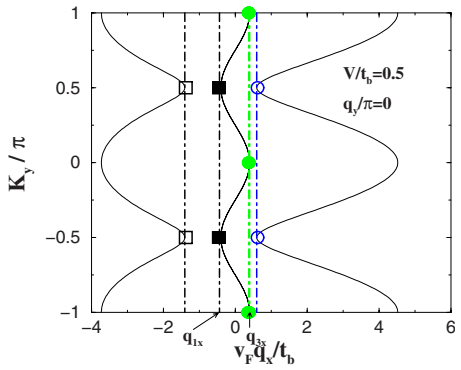

FIG. 13. (Color online) q_x as a function of K_y for $q_y/\pi=0.0$ and $V/t_b=0.5$.

V. NESTING OF THE FERMI SURFACE FOR $V\neq 0$

In this section, we study the effects of periodic potential V on the nesting of the Fermi surface and the susceptibility.

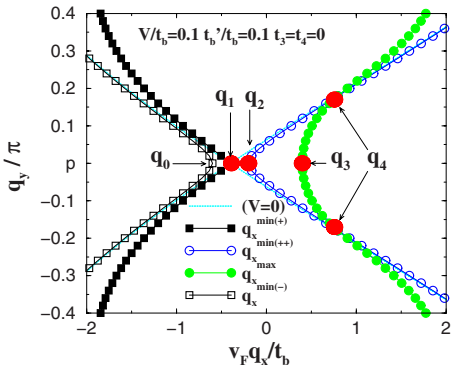

FIG. 14. (Color online) The same as Fig. 5 for $V/t_b=0.1$. q_1 is given as the minimum of $q_x^{(+-)}$ as a function of K_y for each q_y. q_2 is given as $q_x^{(++)}$ at $K_y=\pi/2$ for each q_y. q_3 is given as the maximum of $q_x^{(+-)}$ as a function of K_y for each q_y. q_0 is given as $q_x^{(--)}$ at $K_y=\pi/2$ for each q_y.

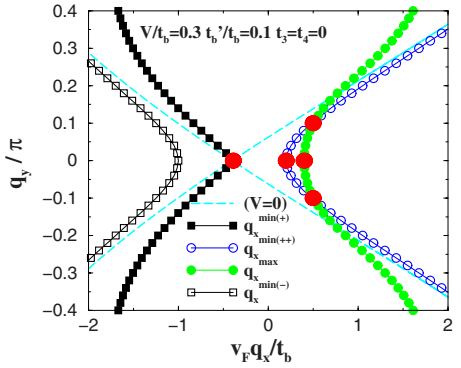

FIG. 15. (Color online) The same as Fig. 14 for $V/t_b=0.3$.

When $V\neq 0$, there are two pairs of the Fermi lines in k_x-k_y plane (see Fig. 2), which are given by k_x as a function of k_y, i.e., $k_x^{L\pm}(k_y)$ and $k_x^{R\pm}(k_y)$ for the left and the right parts of the Fermi lines, respectively. The nesting vectors are characterized into four types according to the pairs of the left and right parts of the Fermi lines, i.e., $(+,-)$, $(-,+)$, $(+,+)$, and $(-,-)$ as shown in Fig. 2. The left and right parts of the Fermi lines are given by

$$k_x^{(L\pm)}(k_y) = -k_F - \frac{1}{v_F}\{-t_\perp(k_y) - t_\perp(k_y+\pi) \pm \sqrt{[t_\perp(k_y)-t_\perp(k_y+\pi)]^2+4V^2}\}, \quad (25)$$

and

$$k_x^{(R\pm)}(k_y) = k_F + \frac{1}{v_F}\{-t_\perp(k_y) - t_\perp(k_y+\pi) \pm \sqrt{[t_\perp(k_y)-t_\perp(k_y+\pi)]^2+4V^2}\}. \quad (26)$$

The condition for the Fermi surface intersects by the translation of the left part [Eq. (11) for $V=0$] is written as the four equations (++, +−, −+, and −−),

$$q_x^{(\pm\pm)} = \frac{1}{2v_F}\{-t_\perp(k_y) - t_\perp(k_y+\pi) - t_\perp(k_y+q_y) - t_\perp(k_y+q_y+\pi) \pm \sqrt{[t_\perp(k_y)-t_\perp(k_y+\pi)]^2+4V^2} \pm \sqrt{[t_\perp(k_y+q_y)-t_\perp(k_y+q_y+\pi)]^2+4V^2}\}. \quad (27)$$

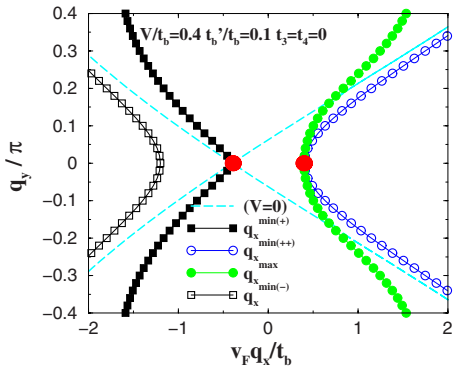

FIG. 16. (Color online) The same as Fig. 14 for $V/t_b=0.4$.

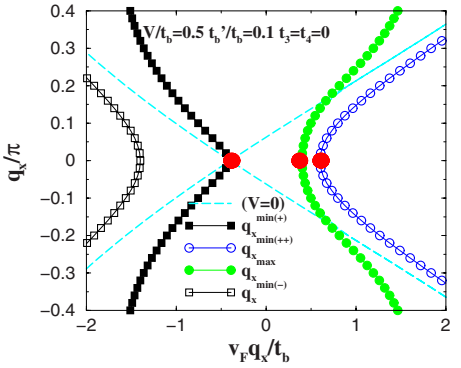

FIG. 17. (Color online) The same as Fig. 14 for $V/t_b=0.5$.

When $q_y=0$, we obtain Eq. (27) for $(+,-)$ and $(-,+)$ to be the same as that for $V=0$ [Eq. (11)],

$$q_x^{(+-)} = q_x^{(-+)} = \frac{1}{v_F}[-t_\perp(k_y) - t_\perp(k_y+\pi)]. \quad (28)$$

The condition for the intersect of $(+,+)$ is obtained as

$$q_x^{(++)} = \frac{1}{v_F}[-t_\perp(k_y) - t_\perp(k_y+\pi)] + \frac{1}{v_F}\sqrt{[t_\perp(k_y)-t_\perp(k_y+\pi)]^2+4V^2}, \quad (29)$$

and the condition for the intersect of $(--)$ is obtained as

$$q_x^{(--)} = \frac{1}{v_F}[-t_\perp(k_y) - t_\perp(k_y+\pi)] - \frac{1}{v_F}\sqrt{[t_\perp(k_y)-t_\perp(k_y+\pi)]^2+4V^2}. \quad (30)$$

We define q_{0x}, q_{1x}, q_{2x}, and q_{3x} as the maximum of $q_x^{(--)}$ (at $K_y=\pm\pi/2$), the minimum of $q_x^{(+-)}$ (at $K_y=\pm\pi/2$), the minimum of $q_x^{(++)}$ (at $K_y=\pm\pi/2$), and the maximum of $q_x^{(+-)}$ (at $K_y=0$ and π) as a function of K_y when $q_y=0$ ($q_{0y}=q_{1y}=q_{2y}=q_{3y}=0$), respectively (see Fig. 10), i.e.,

$$\mathbf{q}_0 = \left(\frac{1}{v_F}(-4t_b'+4t_4-2V),0\right), \quad (31)$$

$$\mathbf{q}_1 = \left(\frac{1}{v_F}(-4t_b'+4t_4),0\right), \quad (32)$$

$$\mathbf{q}_2 = \left(\frac{1}{v_F}(-4t_b'+4t_4+2V),0\right), \quad (33)$$

$$\mathbf{q}_3 = \left(\frac{1}{v_F}(4t_b'+4t_4),0\right). \quad (34)$$

When q_y is given, the maximums and minimums of $q_x^{(+-)}$ are obtained as a function of K_y as shown by the filled green circles and the filled squares in Figs. 10–13. We define $q_x^{\max}(q_y)$ and $q_x^{\min(+)}(q_y)$ by the maximums (filled green circles) and minimums (filled squares) of $q_x^{(+-)}$ for each q_y, respectively. We also define $q_x^{\min(-)}(q_y)$ by the value of $q_x^{(--)}$

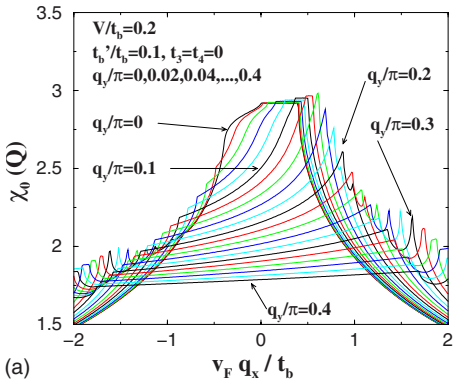

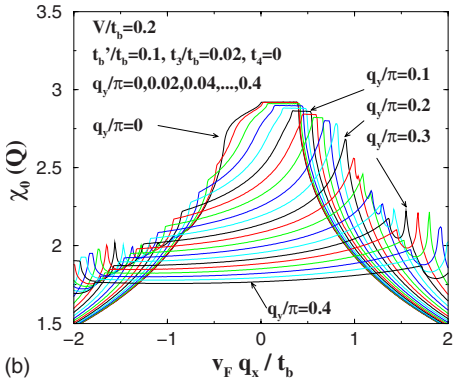

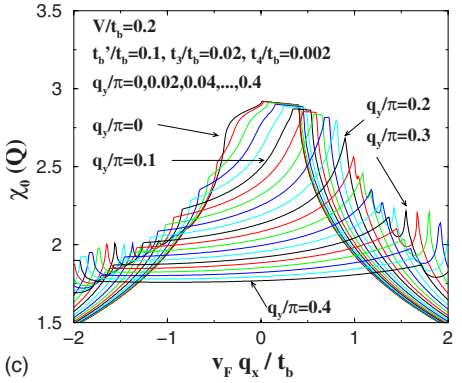

FIG. 18. (Color online) $\chi_0(\mathbf{Q})$ at $T=0$ as a function of q_x. The parameters are the same as in Fig. 6 but $V/t_b=0.2$.

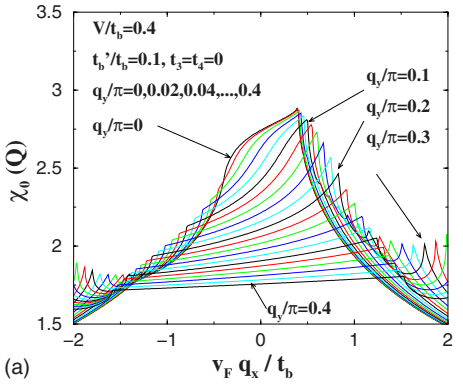

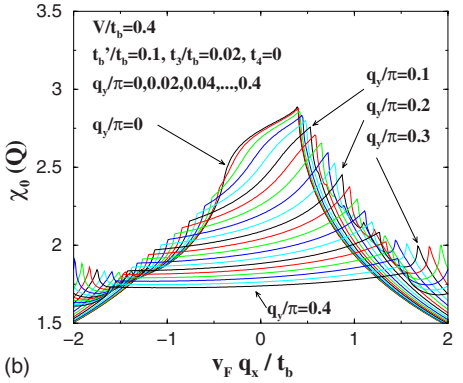

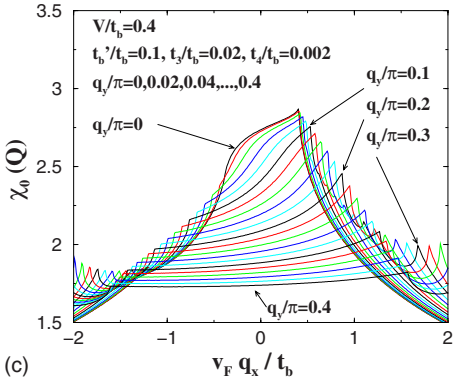

FIG. 19. (Color online) The same as Fig. 18 with $V/t_b=0.4$.

at $K_y=\pm\pi/2$ (open black squares) and $q_x^{\min(++)}(q_y)$ by the value of $q_x^{(++)}$ at $K_y=\pm\pi/2$ (open circles). In Figs. 14–17 we plot $q_x^{\max}(q_y)$, $q_x^{\min(+)}(q_y)$, $q_x^{\min(-)}(q_y)$, and $q_x^{\min(++)}(q_y)$ in the planes of q_x and q_y for $V/t_b=0.1$, 0.3, 0.4, and 0.5. As V becomes zero, $q_x^{\min(++)}(q_y)$, $q_x^{\max}(q_y)$, and $q_x^{\min(-)}(q_y)$ approach to $q_x^{\min(+)}(q_y)$, $q_x^{\max}(q_y)$, and $q_x^{\min(-)}(q_y)$ at $V=0$, respectively (cf. Fig. 5). On the other hand, $q_x^{\min(+)}(q_y)$ has no partner at $V=0$, since the filled squares in Figs. 10–13 become not the minimum but just the crossing points due to the folding in K_y as V becomes zero. We define $\mathbf{q}_4$ as the crossing points of $q_x^{\min(++)}(q_y)$ and $q_x^{\max}(q_y)$, which is the extension of that in $V=0$.

We plot $\chi_0(\mathbf{Q}_0+\mathbf{q})$ as a function of q_x for several values of q_y in Fig. 18 ($V/t_b=0.2$) and Fig. 19 ($V/t_b=0.4$) for the parameters $t_b'/t_b=0.1$ and some values of t_3 and t_4. The contour plots of $\chi_0(\mathbf{Q}_0+\mathbf{q})$ in the k_x-k_y plane are shown in Fig. 20 ($t_3=t_4=0$) and Fig. 21 ($t_3/t_b=0.02$, $t_4/t_b=0.002$) for $V/t_b=0$, 0.2 ($V/t_b'=2$), and 0.4 ($V/t_b'=4$). When $0<V<4t_b'$, $q_{1x}<q_{2x}<q_{3x}$. In this case $\chi_0(\mathbf{Q}_0+\mathbf{q})$ has a plateaulike maximum in the *sweptback* region enclosed by $\mathbf{q}_2$, $\mathbf{q}_4$, and $\mathbf{q}_3$ as shown in Figs. 14 and 15. This region shrinks to the point $\mathbf{q}_3$ when $V/t_b'=4$ as shown in Fig. 16. The absolute maximum of $\chi_0(\mathbf{Q}_0+\mathbf{q})$ occurs near $\mathbf{q}_4$ if $t_3=t_4=0$. The effects of t_3 and t_4 on $\chi_0(\mathbf{Q}_0+\mathbf{q})$ are the same as those at $V=0$. A finite t_3 suppresses $\chi_0(\mathbf{Q}_0+\mathbf{q})$ at $q_y\neq 0$ and t_4 lifts the degeneracy at $q_{2x}\leq q_x\leq q_{4x}$. If $V>4t_b'$, we obtain $q_{1x}<q_{3x}<q_{2x}$ and there is no region where $\chi_0(\mathbf{Q})$ has a plateaulike maximum as shown in Figs. 16, 17, and 19. In that case, the effects of t_3 and t_4 are small. In Fig. 22, $\mathbf{q}_2$ and $\mathbf{q}$ which gives the maximum of $\chi_0(\mathbf{Q}_0+\mathbf{q})$ (i.e., the best nesting vector) are shown for some values of V/t_b in the case of $t_3=t_4=0$. The best nesting vector moves to $\mathbf{q}_3$ as V/t_b approaches 0.4.

The negative Hall constant in some region of the magnetic field[38,39] has been explained by the t_3 and t_4 terms.[15] When $V=0$, the terms with $t_3/t_b=0.02$ and $t_4/t_b=0.002$ make

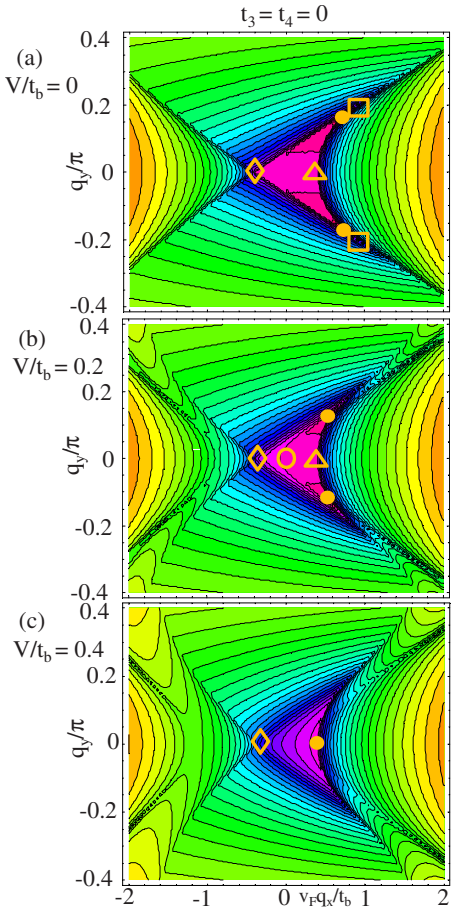

FIG. 20. (Color online) The contour plot of $\chi_0(\mathbf{Q}_0+\mathbf{q})$. The filled circles show the location of the maximum (best nesting vector). The diamonds, the open circles, the triangles, and the squares are $\mathbf{q}_1$, $\mathbf{q}_2$, $\mathbf{q}_3$, and $\mathbf{q}_4$, respectively. We take $t_b'/t_b=0.1$ and $t_3=t_4=0$.

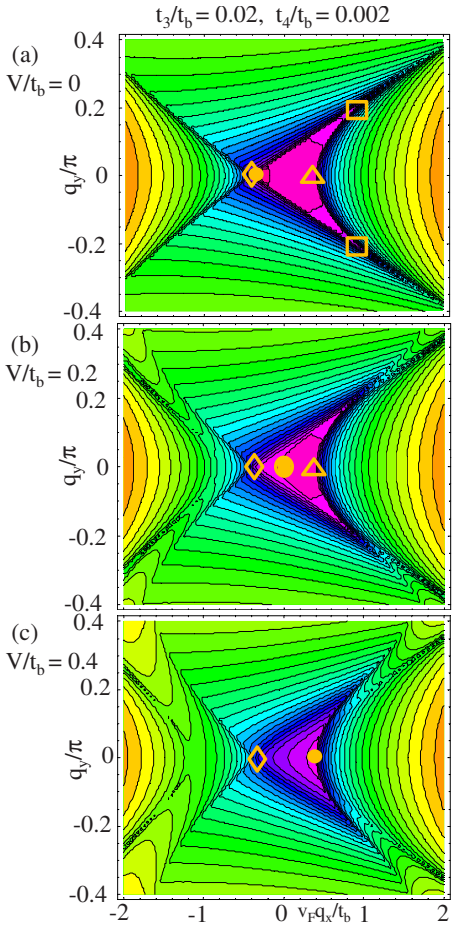

FIG. 21. (Color online) The same as Fig. 20 with $t_b'/t_b=0.1$, $t_3/t_b=0.02$, and $t_4/t_b=0.002$.

the absolute maximum of $\chi_0(\mathbf{Q})$ in the zero magnetic field to be at $\mathbf{q}_1$ (best nesting vector), while the best nesting vector is located near $\mathbf{q}_4$ if $t_3=t_4=0$ as shown in Fig. 6. The negative Hall constant is possible since $q_{1x}<0$. If $V/t_b'>0$ and t_3 and t_4 are the same as above, the best nesting vector is $\mathbf{q}_2$ (see the lower figures in Fig. 18 and the middle figure in Fig. 21). As far as $V<2t_b'-2t_4$, the negative Hall constant is possible since $q_{2x}<0$. If $V>2t_b'-2t_4$, however, the best nesting vector $\mathbf{q}_2$ has the positive x component as seen in the lower figures in Figs. 18 and 19. Therefore, the negative Hall constant is difficult to be stabilized when $V>2t_b'-2t_4$. Recently, the authors[33] have numerically obtained the phase diagram for the quantum Hall effect as a function of the magnetic field and periodic potential V. We have shown that the negative Hall constant ($N=-2$) appears only in the region $0.03 \lesssim V/t_b \lesssim 0.2$ ($0.3 \lesssim V/t_b' \lesssim 2$) for the parameters $t_b'/t_b=0.1$, $t_3/t_b=0.02$, and $t_4/t_b=0.002$ (the upper figure of Fig. 12 in Ref. 33). That result can be understood by the fact that for $V>2t_b'-2t_4$ the best nesting vector has the positive x component. The existence of the negative Hall constant for $V/t_b' \gtrsim 0.3$ is understood by the effect of V that will make $\chi_0(\mathbf{Q}_0+\mathbf{q})$ at $\mathbf{q} \approx \mathbf{q}_4$ smaller. Experimentally, a negative Hall effect is observed when the system is cooled slowly (less than 0.03 K/s) and the external magnetic-field region for the negative Hall effect becomes larger as the cooling rate becomes slower (the slowest cooling rate is 0.000 09 K/s) (Ref. 38). It is expected that the magnitude of the periodic potential V becomes larger at the slower cooling rate. Therefore, we can conclude from the existence of the negative Hall effect in $(TMTSF)_2ClO_4$ that $V<2t_b'-2t_4$. The value of V estimated from the magnetic-field-angle dependence of the conductivity[34–36] is close to the border of this condition.

VI. SUMMARY AND DISCUSSIONS

We have studied the nesting vector and $\chi_0(\mathbf{Q})$ in the quasi-one-dimensional systems having the imperfectly nested Fermi surface (the imperfectness is measured by t_b'). We have obtained the plateaulike maximum of $\chi_0(\mathbf{Q})$ when $\mathbf{Q}$ is in the *sweptback* region with the apexes $\mathbf{q}_1$ and $\mathbf{q}_4$. The absolute maximum of $\chi_0(\mathbf{Q})$ is obtained near but not at $\mathbf{Q}=\mathbf{Q}_0+\mathbf{q}_4$ if $t_3=t_4=0$. When the periodic potential V is finite but not as large as $4t_b'$ [which is thought to be the case in $(TMTSF)_2ClO_4$], the sweptback region (with apexes $\mathbf{q}_2$ and $\mathbf{q}_4$) becomes smaller as V increases and shrinks to $\mathbf{q}_3$ when $V=4t_b'$. The best nesting vector moves to $\mathbf{Q} \approx \mathbf{Q}_0+\mathbf{q}_3$. The absolute maximum of $\chi_0(\mathbf{Q})$ is located at $\mathbf{Q}=\mathbf{Q}_0+\mathbf{q}_3$ when $V>4t_b'$. The negative Hall coefficient observed in the field-

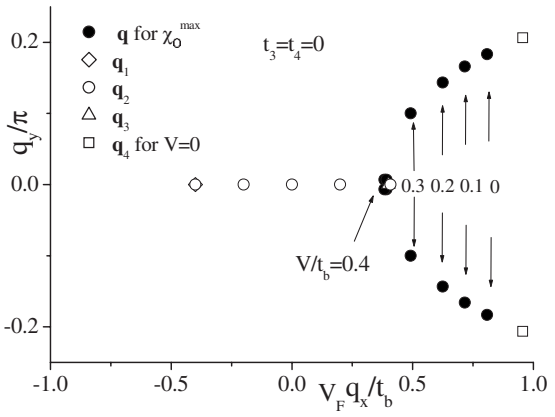

FIG. 22. Open diamond, open triangle, and open squares are $\mathbf{q}_1$, $\mathbf{q}_3$, and $\mathbf{q}_4$ for $V=0$, respectively. Open circles and closed circles are $\mathbf{q}_2$ and the locations of the maximum of $\chi_0(\mathbf{Q})$ (best nesting vector), respectively, for $V/t_b=0$, 0.1, 0.2, 0.3, and 0.4. We take $t_b'/t_b=0.1$ and $t_3=t_4=0$.

induced spin-density wave states in some region of the magnetic field is shown to be possible only when $V<2t_b'-2t_4$, in which case the vectors $\mathbf{q}$'s giving the plateaulike maximum of $\chi_0(\mathbf{Q}_0+\mathbf{q})$ (*sweptback* region) can have the negative x component ($q_{2x}<0$). Therefore, we conclude that V should be smaller than $2t_b'-2t_4$ in $(TMTSF)_2ClO_4$, where the sign reversal of the Hall effect has been observed.

Recently, a lot of interest is attracted by the quasi-one-dimensional conductor $(Per)_2M(mnt)_2$ (where Per=perylene, mnt=maleonitriledithiolate, and M=Au and Pt) (Refs. 42–46). The charge-density wave (CDW) state is realized in $(Per)_2M(mnt)_2$ and the successive transitions of the field-induced CDW has been observed in high magnetic field[42] in contrast to the field-induced SDW in $(TMTSF)_2ClO_4$. This material has a similar band structure as $(TMTSF)_2ClO_4$, but the origin of the pairs of the quasi-one-dimensional Fermi surface in $(Per)_2M(mnt)_2$ is different from that in $(TMTSF)_2ClO_4$. The origin of the four pairs of the quasi-one-dimensional Fermi surface in $(Per)_2M(mnt)_2$ is the existence of four perylene molecules in the unit cell in the perpendicular plane to the conduction axis,[46] while the origin of the two pairs of the quasi-one-dimensional Fermi surface in $(TMTSF)_2ClO_4$ is the periodic potential caused by the anion ordering. It will be interesting to study the similarity and the difference between the two materials, since the spin susceptibility $\chi_0(\mathbf{Q})$ and the charge susceptibility $\chi_c(\mathbf{Q})$ for the noninteracting system have the same $\mathbf{Q}$ dependence caused by the nesting properties of the Fermi surface, except for the effects of the Zeeman splitting of the Fermi surface, which play an important role only for CDW.

ACKNOWLEDGMENTS

This work was partly supported by a Grant-in-Aid for the Promotion of Science and Scientific Research on Priority Areas (Grant No. 18028021) from the Ministry of Education, Culture, Sports, Science and Technology, Japan.

[1] For a review, see, T. Ishiguro, K. Yamaji, and G. Saito, *Organic Superconductors*, 2nd ed. (Springer-Verlag, Berlin, 1998); *The Physics of Organic Superconductors and Conductors*, edited by A. G. Lebed (Springer, New York, 2008).
[2] L. P. Gor'kov and A. G. Lebed', J. Phys. (Paris), Lett. **45**, 433 (1984).
[3] G. Montambaux, M. Heritier, and P. Lederer, Phys. Rev. Lett. **55**, 2078 (1985).
[4] K. Yamaji, J. Phys. Soc. Jpn. **54**, 1034 (1985).
[5] A. G. Lebed', Sov. Phys. JETP **62**, 595 (1985).
[6] K. Maki, Phys. Rev. B **33**, 4826 (1986).
[7] A. Virosztek, L. Chen, and K. Maki, Phys. Rev. B **34**, 3371 (1986).
[8] L. Chen and K. Maki, Phys. Rev. B **35**, 8462 (1987).
[9] K. Yamaji, J. Phys. Soc. Jpn. **56**, 1841 (1987).
[10] K. Machida, Y. Hori, and M. Nakano, Phys. Rev. Lett. **70**, 61 (1993).
[11] A. G. Lebed, Phys. Rev. Lett. **88**, 177001 (2002).
[12] D. Poilblanc, G. Montambaux, M. Heritier, and P. Lederer, Phys. Rev. Lett. **58**, 270 (1987).
[13] V. M. Yakovenko, Phys. Rev. B **43**, 11353 (1991).
[14] K. Machida, Y. Hasegawa, M. Kohmoto, V. M. Yakovenko, Y. Hori, and K. Kishigi, Phys. Rev. B **50**, 921 (1994).
[15] D. Zanchi and G. Montambaux, Phys. Rev. Lett. **77**, 366 (1996).
[16] N. Dupuis and V. M. Yakovenko, Phys. Rev. Lett. **80**, 3618 (1998).
[17] J. F. Kwak, J. E. Schirber, R. L. Greene, and E. M. Engler, Phys. Rev. Lett. **46**, 1296 (1981).
[18] P. M. Chaikin, M. Y. Choi, J. F. Kwak, J. S. Brooks, K. P. Martin, M. J. Naughton, E. M. Engler, and R. L. Greene, Phys. Rev. Lett. **51**, 2333 (1983).
[19] M. Ribault, D. Jerome, J. Tuchendler, C. Weyl, and K. Bechgaard, J. Phys. (Paris), Lett. **44**, L953 (1983).
[20] M. J. Naughton, J. S. Brooks, L. Y. Chiang, R. V. Chamberlin, and P. M. Chaikin, Phys. Rev. Lett. **55**, 969 (1985).
[21] W. Kang, S. T. Hannahs, and P. M. Chaikin, Phys. Rev. Lett. **70**, 3091 (1993).
[22] S. K. McKernan, S. T. Hannahs, U. M. Scheven, G. M. Danner, and P. M. Chaikin, Phys. Rev. Lett. **75**, 1630 (1995).
[23] U. M. Scheven, E. I. Chashechkina, E. Lee, and P. M. Chaikin, Phys. Rev. B **52**, 3484 (1995).
[24] N. Matsunaga, A. Ayari, P. Monceau, A. Ishikawa, K. Nomura, M. Watanabe, J. Yamada, and S. Nakatsuji, Phys. Rev. B **66**, 024425 (2002).
[25] A. G. Lebed and P. Bak, Phys. Rev. B **40**, 11433 (1989).
[26] T. Osada, S. Kagoshima, and N. Miura, Phys. Rev. Lett. **69**, 1117 (1992).
[27] H. Yoshino, A. Oda, T. Sasaki, T. Hanajiri, J. Yamada, S. Nakatsuji, H. Anzai, and K. Murata, J. Phys. Soc. Jpn. **68**, 3142 (1999).
[28] M. Miyazaki, K. Kishigi, and Y. Hasegawa, J. Phys. Soc. Jpn. **68**, 313 (1999).

[29] K. Sengupta and N. Dupuis, Phys. Rev. B **65**, 035108 (2001).
[30] D. Zanchi and A. Bjelis, Europhys. Lett. **56**, 596 (2001).
[31] S. Haddad, S. Charfi-Kaddour, M. Heritier, and R. Bennaceur, Phys. Rev. B **72**, 085104 (2005).
[32] Y. Hasegawa, K. Kishigi, and M. Miyazaki, J. Phys. Soc. Jpn. **67**, 964 (1998).
[33] K. Kishigi and Y. Hasegawa, Phys. Rev. B **75**, 245107 (2007).
[34] H. Yoshino, S. Shodai, and K. Murata, Synth. Met. **133-134**, 55 (2003).
[35] A. G. Lebed, Heon-Ick Ha, and M. J. Naughton, Phys. Rev. B **71**, 132504 (2005).
[36] H. I. Ha, A. G. Lebed, and M. J. Naughton, Phys. Rev. B **73**, 033107 (2006).
[37] K. Yamaji, J. Phys. Soc. Jpn. **55**, 860 (1986).
[38] N. Matsunaga, K. Hino, T. Ohta, K. Yamashita, K. Nomura, T. Sasaki, A. Ayari, P. Monceau, M. Watanabe, J. Yamada, and S. Nakatsuji, J. Phys. (Paris) IV **131**, 269 (2005).
[39] M. Ribault, Mol. Cryst. Liq. Cryst. **119**, 91 (1985).
[40] K. Kishigi, K. Machida, and Y. Hasegawa, J. Phys. Soc. Jpn. **66**, 2969 (1997).
[41] K. Kishigi, J. Phys. Soc. Jpn. **67**, 3825 (1998).
[42] D. Graf, E. S. Choi, J. S. Brooks, R. T. Henriques, M. Almeida, and M. Matos, Phys. Rev. Lett. **93**, 076406 (2004).
[43] R. D. McDonald, N. Harrison, J. Singleton, A. Bangura, P. A. Goddard, A. P. Ramirez, and X. Chi, Phys. Rev. Lett. **94**, 106404 (2005).
[44] A. G. Lebed and S. Wu, Phys. Rev. Lett. **99**, 026402 (2007).
[45] D. Graf, J. S. Brooks, E. S. Choi, M. Almeida, R. T. Henriques, J. C. Dias, and S. Uji, Phys. Rev. B **75**, 245101 (2007).
[46] E. Canadell, M. Almeida, and J. Brooks, Eur. Phys. J. B **42**, 453 (2004).